Atmos. Meas. Tech. Discuss., doi:10.5194/amt-2017-65, 2017
Manuscript under review for journal Atmos. Meas. Tech.
Discussion started: 18 April 2017

Atmospheric Measurement Techniques Discussions

Aethalometer multiple scattering correction C_{ref} for mineral dust aerosols

Claudia Di Biagio[1], Paola Formenti[1], Mathieu Cazaunau[1], Edouard Pangui[1], Nicholas Marchand[2], and Jean-François Doussin[1]

[1] Laboratoire Interuniversitaire des Systèmes Atmosphériques (LISA), UMR 7583, CNRS, Université Paris Est Créteil et Université Paris Diderot, Institut Pierre et Simon Laplace, Créteil, France

[2] Aix Marseille Université, CNRS, LCE, Marseille, France

Correspondence to: C. Di Biagio (cldibiagio@gmail.com) and P. Formenti (paola.formenti@lisa.u-pec.fr)

Abstract

In this study we provide a first estimate of the aethalometer multiple scattering correction C_{ref} for mineral dust aerosols. The C_{ref} at 450 and 660 nm was obtained from the direct comparison of aethalometer data (Magee Sci. AE31) with the absorption coefficient calculated as the difference between the extinction and scattering coefficients measured by a CAPS PMex and a nephelometer at 450 nm and the absorption coefficient from a MAAP (Multi-Angle Absorption Photometer) at 660 nm. Measurements were performed on seven dust aerosol samples generated in the laboratory by the mechanical shaking of natural parent soils issued from different source regions worldwide. The single scattering albedo (SSA) at 450 and 660 nm and the size distribution of the aerosols were also measured.

C_{ref} for mineral dust varies between 1.81 and 2.56 for a SSA of 0.85–0.96 at 450 nm and between 1.75 and 2.28 for a SSA of 0.98–0.99 at 660 nm. The calculated mean C_{ref} for dust is 2.09 (± 0.22) at 450 nm and 1.92 (± 0.17) at 660 nm. With this new C_{ref} the dust absorption coefficient by aethalometer is about 2% (450 nm) and 11% (660 nm) higher than that obtained by using C_{ref}=2.14, usually assumed in the literature. This difference induces up to 3% change in the dust SSA. The C_{ref} seems independent of the particle fine and coarse size fractions, and so the obtained C_{ref} can be applied to dust both close to sources and following transport. Additional experiments performed with pure kaolinite mineral and polluted ambient aerosols indicate a C_{ref} of 2.49 (± 0.02) and 2.32 (± 0.01) at 450 and 660 nm (SSA=0.96–0.97) for kaolinite, and a C_{ref} of 2.32 (± 0.36) at 450 nm and 2.32 (± 0.35) at 660 nm for pollution aerosols (SSA=0.62–0.87 at 450 nm and 0.42–0.76 at 660 nm).

Atmos. Meas. Tech. Discuss., doi:10.5194/amt-2017-65, 2017
Manuscript under review for journal Atmos. Meas. Tech.
Discussion started: 18 April 2017

Atmospheric Measurement Techniques Discussions

1. Introduction

Abundant and widespread in the atmosphere, mineral dust strongly contributes to the global and regional direct radiative effect and climate forcing (Highwood and Ryder, 2014; Miller et al., 2014). Mineral dust interacts through processes of scattering and absorption with both incoming shortwave radiation and outgoing terrestrial longwave radiation (Sokolik et al., 1999). As for today, the evaluation of the direct effect of mineral dust and its climate implications is still limited by the knowledge of the intensity of the dust absorption in the shortwave spectral range (Miller et al., 2004; Balkanski et al., 2007; Solmon et al., 2008; Jin et al., 2016), represented by the light absorption coefficient (β_{abs}, units of Mm^{-1}). The absorption coefficient of mineral dust accounts for less than ~10-20% of its total shortwave extinction, where it shows a pronounced spectral variation (Cattrall et al., 2003; Redmond et al., 2010). The highest dust absorption occurs in the UV-VIS region of the spectrum, while it levels off to null values towards the near IR (Caponi et al., 2017). As a result, its single scattering albedo (SSA), i.e. the ratio of the aerosol scattering (β_{sca}) to extinction ($\beta_{ext}=\beta_{sca}+\beta_{abs}$) coefficient, increases from values of ~0.80-0.90 at 370 nm to values of ~0.95-0.99 at 950 nm (e.g., Schladitz et al., 2009; Redmond et al., 2010; Formenti et al., 2011; Ryder et al., 2013).

Given its relatively high SSA, mineral dust can be considered as weakly absorbing in the shortwave. This is particularly true if compared to other aerosol species as soot for which the SSA in the visible may be as low as 0.2 (Bergstrom et al., 2007). Nonetheless, because of its elevated atmospheric concentration (~100÷100000 μg m^{-3} close to sources and ~0.1÷100 μg m^{-3} after mid– to intercontinental transport; e.g., Goudie and Middleton, 2006; Kandler et al., 2009; Querol et al., 2009; Denjean et al., 2016a), light absorption by mineral dust can be comparable to that of soot both at regional and global scale (Reddy et al., 2005; Caponi et al., 2017). Under very intense dust episodes, dust may absorb up to ~150 Wm^{-2} of incoming solar radiation (Slingo et al., 2006; di Sarra et al., 2011), inducing a remarkable warming of the atmospheric layer. This strong warming can alter the atmospheric structure and stability (Heinold et al., 2008), with a possible influence on the atmospheric dynamics and meteorological fields (Pérez et al., 2006). By its direct shortwave effect dust also affects the position of the Inter Tropical Convergence Zone, which in turn influences the Western African Monsoon and modifies the pattern and intensity of rainfall over Northern Africa and the Sahel (Yoshioka et al., 2007). Nonetheless, the extent of the dust effect and its implications critically depend on the exact amount of absorbed shortwave radiation. Solmon et al. (2008), for example, showed that a small change (5%) in the shortwave SSA of dust may modify the effect of dust on the Western African Monsoon, moving from a reduction to an increase of precipitation over the Sahel.

The accurate estimation of the dust absorption over the whole shortwave range is therefore necessary to properly assess its direct radiative effect and climate implications. One instrument measuring the aerosol-light absorption from the UV to near IR range is the aethalometer (Magee Sci. AE31 model, Hansen et al., 1984; Arnott et al., 2005), operating at seven wavelengths in the 370–950 nm range. The aethalometer is used to measure the black carbon mass concentration but the spectral absorption by aerosols can be also calculated. Given its large spectral interval, the aethalometer has been used in the past to investigate the spectral dependence of dust absorption (Fialho et al., 2005;

Atmos. Meas. Tech. Discuss., doi:10.5194/amt-2017-65, 2017
Manuscript under review for journal Atmos. Meas. Tech.
Discussion started: 18 April 2017

Atmospheric Measurement Techniques Discussions

Formenti et al., 2011), as well as the absorption by many aerosol types in different environments (Sandradewi et al., 2008; Segura et al., 2014; Di Biagio et al., 2016; Backman et al., 2016).

The working principle of the aethalometer, a filter-based instrument, consists in measuring the attenuation through an aerosol-laden quartz filter according to the Beer-Lambert law, used then to derive the spectral attenuation coefficient (β_{ATT}) of the deposited particles (Hansen et al., 1984). The "true" spectral aerosol absorption coefficient (β_{abs}) is proportional but lower than β_{ATT} (Weingartner et al., 2003; Collaud Coen et al., 2010; hereinafter referred as W2003 and C2010), because β_{ATT} is enhanced by (i) aerosol scattering towards directions different from that of the detector (scattering effect); (ii) gradual accumulation of absorbing particles on the loaded filter, thus reducing the optical path (shadowing effect); (iii) multiple scattering of the light beam by the filter fibres, increasing the optical path (multiple scattering effect).

Empirical formulations of the scattering and shadowing effects are available in the literature and permit the correction of aethalometer data for these artefacts (W2003; Arnott et al., 2005; Schmid et al., 2006; Virkkula et al., 2007; C2010). The correction of the multiple scattering effect, however requires the knowledge of a correction factor C_{ref}, which needs to be directly estimated by comparison of aethalometer data against reference absorption measurements (W2003; C2010).

Currently data for C_{ref} are available for soot particles (C_{ref}=2.1-2.2 at 660 nm, W2003), internally and externally mixed soot particles and organic material (C_{ref}=2.3-3.9, W2003), and ambient aerosols collected in Europe and Amazonia (C_{ref}=2.6-4.8, C2010; C_{ref}=4.9÷6.3, Saturno et al., 2016) and in the Arctic (C_{ref}=3.1, Backman et al., 2016). The value most often used in the literature is 2.14 (± 0.21), assumed as wavelength-independent (e.g., Sandradewi et al., 2008; Formenti et al., 2011; Di Biagio 2016), which corresponds to the mean of observations at 660 nm for soot aerosols (W2003). Both W2003 and C2010, however, found a dependence of C_{ref} on the aerosol single scattering albedo, with C_{ref} decreasing for increasing SSA. So, the value of 2.14 obtained for highly absorbing soot (SSA~0.2 in the visible) may not be appropriate for weakly absorbing mineral dust.

Henceforth, in this work we present the experimental estimate of an optimized C_{ref} for mineral dust aerosols at 450 and 660 nm obtained from a laboratory-based intercomparison study. Experiments were conducted on seven dust aerosol samples generated by the mechanical shaking of natural parent soils. Control experiments on pure kaolinite mineral, ambient aerosols sampled in the polluted environment of the suburbs of Paris, and purely scattering ammonium sulfate, were also performed to investigate the dependence of C_{ref} on the aerosol single scattering albedo.

2. Experimental set-up

The experimental set-up used for the intercomparison study is shown in **Fig. 1**. The following measurements were performed from a 8-port glass manifold (~1 L volume):

- the absorption coefficient (β_{abs}) by a 7-wavelentgth aethalometer (Magee Sci., model AE31 working at 370, 470, 520, 590, 660, 880, 950 nm; flowrate 8 L min^{-1}, 2-min resolution) and a MAAP (Multi-Angle Absorption Photometer, Thermo Sci., model 5012 working at 670 nm; flowrate 8 L

min^{-1}, 1-min resolution). Unlike the aethalometer, the MAAP measures the transmitted light from the aerosol-laden filter and also the backscattered light at two angles (135° and 165°) (Petzold et al., 2004). Backscattering measurements are used to constrain the scattering fraction of the measured attenuation that would erroneously be interpreted as absorption. The aerosol absorption coefficient for the MAAP is obtained from a radiative transfer scheme taking into account the multiple scattering in the filter and the scattering effect, without requiring any further adjustment (Petzold and Schönlinner, 2004). The MAAP is commonly assumed to provide the most reliable direct estimate of the aerosol absorption coefficient at a single wavelength (Andreae and Gelècser 2006). In this study we assume for the MAAP the manufacturer's reported wavelength of 670 nm, even if Müller et al. (2011) measured for this instrument a wavelength of 637 nm;

- the scattering coefficient (β_{sca}) in the 7-170° angular range by a 3-wavelentgth nephelometer (TSI Inc., model 3563 working at 450, 550 and 700 nm; flowrate 18 L min^{-1}, 1-s resolution);
- the extinction coefficient (β_{ext}) by two Cavity Attenuated Phase Shift Extinction analyzers (CAPS PMex by Aerodyne, one working at 450 nm and the other at 630 nm; flowrate 0.85 L min^{-1}, 1-s resolution);
- the particle number size distribution (dN/dlogD) by a scanning mobility particle sizer, SMPS, (TSI Inc., DMA Model 3080, CPC Model 3772; operated at 2.0/0.2 L min^{-1} sheath/aerosol flow rates; 3-min resolution) and an optical particle counter, OPC, (Grimm Inc., model 1.109, 655 nm operating wavelength; flowrate 1.2 L min^{-1}, 6-s resolution). The SMPS measures the aerosol number concentration in the electrical mobility diameter (D_m) range 0.019–0.882 μm, and the OPC measures in the optical equivalent diameter (D_{opt}) range 0.25-32 μm.

Instrumental details are summarized in **Table 1**.

Sampling lines from the manifold to the instruments were made of conductive silicone tubing (TSI Inc., $6.4 \cdot 10^{-3}$ m diameter) to minimize particle loss by electrostatic deposition. They were designed to be as straight and as short as possible. Their length, varying between 0.3 and 0.7 m, was adjusted based on the flowrate of each instrument to ensure an equivalent particle loss, so the same aerosol size distribution could be assumed as input for all instruments. Particular care was given to ensure the same aerosol size at the input of the aethalometer and the MAAP. To this end, as illustrated in Fig. 1, the two instruments sampled air from the same manifold exit line, and also the same sampling flow rate was set for the two instruments (8 L min^{-1}). Particle loss calculations were performed with the Particle Loss Calculator (PLC) software (von der Weiden et al., 2009).

Aerosols were generated in three ways:

- mineral dust was generated by mechanical shaking as described and validated in Di Biagio et al. (2014, 2017). About 3 gr of soil sample (sieved at 1000 μm and dried at 100°C) was placed in a Büchner flask and shaken at 100 Hz by a sieve shaker (Retsch AS200). The dust was injected in the manifold by a flow of N_2 at 3.5 L min^{-1} through a single-stage impactor used to eliminate particles larger than about 20 μm, which could be preferentially sampled by the instruments with the highest

Atmos. Meas. Tech. Discuss., doi:10.5194/amt-2017-65, 2017
Manuscript under review for journal Atmos. Meas. Tech.
Discussion started: 18 April 2017

Atmospheric Measurement Techniques Discussions

flow rate. Pure N_2 was added to the aerosol flow to make the injection flow equal to the total sampling flow by instruments connected to the manifold (about 38 L min^{-1});

- ammonium sulfate (Sigma-Aldrich 99.999% purity, 0.03 M solution in ultrapure water) and kaolinite particles (Source Clay Repository KGa-2, 0.05 M solution in ultrapure water) were generated by a constant flow atomizer (TSI, model 3075) operated at 3 L min^{-1} and coupled with a diffusion drier (TSI, model 3062). As for dust, pure N_2 was added to the aerosol flow to equalize the total sampling flow;

- ambient pollution aerosols were sampled by opening the manifold to the exterior ambient air. Sampling was performed at the University Paris-Est Creteil, in the suburbs of Paris, at the ground floor of the University building, which is close to a main local road (~20 m) and to the A86 highway (~200 m).

3. Strategy for data analysis

The aethalometer spectral attenuation coefficient $\beta_{ATT}(\lambda)$ is related to the measured attenuation ATT(λ) through the following formula:

$$\beta_{ATT}(\lambda) = \frac{\Delta ATT(\lambda)}{\Delta t}\frac{A}{V} \quad (1)$$

where A is the area of the aerosol collection spot (0.5 ± 0.1) cm^2 and V the air sampled volume (0.016 m^3 over 2-min integration time). $\Delta ATT(\lambda)/\Delta t$ in Eq. (1) can be calculated as the linear fit of the measured attenuation as a function of time.

The spectral attenuation coefficient $\beta_{ATT}(\lambda)$ measured by the aethalometer is related to the targeted absorption coefficient $\beta_{abs}(\lambda)$ by the following formula (C2010):

$$\beta_{abs}(\lambda) = \frac{\beta_{ATT}(\lambda) - \alpha(\lambda)\beta_{sca}(\lambda)}{R \cdot C_{ref}} \quad (2)$$

where the different terms parametrise different instrument artefacts:

- the scattering effect $\alpha(\lambda)\beta_{sca}(\lambda)$, that is, the amount of scattered radiation by the aerosols deposited on the filter that is miscounted as absorption, where α(λ) is a wavelength-dependent proportionality constant and $\beta_{sca}(\lambda)$ is the aerosol spectral scattering coefficient;

- the shadowing effect R, representing the artificial flattening of measured attenuation with time due to the gradual accumulation of absorbing particles on the loaded filter;

- the multiple scattering C_{ref}, representing multiple scattering of the light beam by the filter fibres.

The α(λ) term and R in Eq. (2) can be calculated through various empirical formulas reported in the literature (W2003, Arnott et al., 2005; Virkkula et al., 2007; Schmid et al., 2006; C2010). The determination of C_{ref},instead, is the objective of our study.

Atmos. Meas. Tech. Discuss., doi:10.5194/amt-2017-65, 2017
Manuscript under review for journal Atmos. Meas. Tech.
Discussion started: 18 April 2017

Atmospheric Measurement Techniques Discussions

3.1. Scattering effect correction

Arnott et al. (2005) provide for α(λ) the following formulation:

$$\alpha(\lambda)=A^{d-1}\cdot c\cdot\lambda^{-\alpha_S(d-1)} \quad (3)$$

where the A and α_S terms are obtained from the power-law fit of $\beta_{sca}(\lambda)$ versus λ, and the c and d terms can be determined from the power-law fit of the attenuation $\beta_{ATT}(\lambda)$ versus the scattering $\beta_{sca}(\lambda)$ coefficient as

$$\beta_{sca}(\lambda)=A\lambda^{-\alpha_S} \quad (4)$$

$$\beta_{ATT}(\lambda)=c\beta_{sca}(\lambda)^{d} \quad (5)$$

3.2. Shadowing effect correction

Two formulations for the shadowing effect correction R are proposed by W2003 and C2010:

$$R(W2003)(\lambda)=\left(\frac{1}{f(\lambda)}-1\right)\frac{\ln(ATN(\lambda))-\ln(10\%)}{\ln(50\%)-\ln(10\%)}+1 \quad (6a)$$

$$R(C2010)(\lambda)=\left(\frac{1}{f(\lambda)}-1\right)\frac{ATN(\lambda)}{50\%}+1 \quad (6b)$$

The factor f(λ) represents the dependence of the shadowing effect on the aerosol absorption. This dependence is parametrized by the aerosol single scattering albedo SSA(λ) in the form of

$$f(\lambda)=a(1-SSA(\lambda))+1 \quad (7)$$

where *a*, equal to 0.85 in W2003 and 0.74 in C2010, is obtained as the slope of the linear fit between the attenuation coefficient β_{ATT} normalized to its value at 10% attenuation ($\beta_{ATT}/\beta_{10\%}$) and the natural logarithm of the measured attenuation ln(ATT(λ)).

3.3. Multiple scattering correction

For the determination of C_{ref} only β_{ATT} and R are required. Henceforth in this work, attenuation data from the aethalometer were corrected for the shadowing effect R but not for the scattering term $\alpha(\lambda)\beta_{sca}(\lambda)$. Three different formulations of C_{ref} were therefore considered:

$$C_{ref}^{*}(\lambda)=\frac{\beta_{ATT}(\lambda)}{\beta_{abs\text{-}ref}(\lambda)} \quad (8a)$$

$$C_{ref}(W2003)(\lambda)=\frac{1}{\beta_{abs\text{-}ref}(\lambda)}\frac{\beta_{ATT}(\lambda)}{R(W2003)(\lambda)} \quad (8b)$$

$$C_{ref}(C2010)(\lambda)=\frac{1}{\beta_{abs\text{-}ref}(\lambda)}\frac{\beta_{ATT}(\lambda)}{R(C2010)(\lambda)} \quad (8c)$$

Atmos. Meas. Tech. Discuss., doi:10.5194/amt-2017-65, 2017
Manuscript under review for journal Atmos. Meas. Tech.
Discussion started: 18 April 2017

Atmospheric Measurement Techniques Discussions

The $\beta_{abs\text{-}ref}$ term in Eq. 8a-8c represents the reference absorption coefficient estimated from independent measurements. C_{ref}^{*} does not take into account the shadowing effect correction in aethalometer data, as done by Schmid et al. (2006). C_{ref}(W2003) and C_{ref}(C2010) take this correction into account, by using the R(W2003) and the R(C2010) parametrisations, respectively. The spectral β_{ATT}/R(C2010) was used to calculate the absorption Ángström exponent (α_A). Note that in this work we considered, for each experiment, only data corresponding to ATT < 20% to calculate β_{ATT} (R^2>0.99 for the ΔATT/Δt fits in all cases, see Eq. (1)). This threshold was fixed based on two requirements: first, we limited our data analysis to points with low attenuation in order to account almost exclusively for the scattering by the filter fibers in the C_{ref} calculation and not for the scattering from aerosol particles embedded in the filter. This choice was done also for consistency with the literature, since both W2003 and C2010 relate C_{ref} to ATT~10%. Second, this choice ensured that enough data points were available for analysis regardless of the aerosol type, in particular for ambient aerosols, for which attenuation rapidly exceeded 10%.

3.4. Determination of reference absorption coefficient and single scattering albedo

The reference absorption coefficient $\beta_{abs\text{-}ref}$ in Eq. 8a-8c was obtained in different ways depending on wavelength. At 450 nm, $\beta_{abs\text{-}ref}$ was obtained with the “extinction minus scattering” approach by using the CAPS measurements for extinction and the nephelometer measurements for scattering. At 660 nm, $\beta_{abs\text{-}ref}$ was extrapolated from MAAP measurements at 670 nm.

3.4.1. Direct determination of reference absorption coefficient at 660 nm from the MAAP

The reference absorption coefficient $\beta_{abs\text{-}ref}$ at 660 nm was obtained by the MAAP measurement at 670 nm. The MAAP attenuation (ATT) at 670 nm is estimated from the measured transmission (T) and retrieved single scattering albedo of the aerosol-filter layer (SSA_0, from the inversion algorithm) as

$$ATT(670) = (1 - SSA_0) \cdot \ln T \cdot 100 \quad (9)$$

Equation (1) is applied to estimate the absorption coefficient at 670 nm from ATT(670). The area of the aerosol collection spot is 2 cm^2 and the sampled volume is 0.008 m^3 over 1-min integration time. The absorption coefficient of the MAAP was extrapolated to the 660 nm wavelength by using the absorption Ángström exponent α_A calculated from aethalometer data.

3.4.2. Indirect determination of reference absorption coefficient at 450 nm: "extinction minus scattering” approach

The reference absorption coefficient $\beta_{abs\text{-}ref}$ at 450 nm was calculated as the difference between the extinction and scattering coefficient from the CAPS and the nephelometer.

The extinction coefficient β_{ext} at 450 and 630 nm was measured directly by the two CAPS analyzers without additional corrections (Massoli et al., 2010). The spectral β_{ext} was used to calculate the extinction Ángström exponent (α_E), applied then to extrapolate β_{ext} at 660 nm.

Atmos. Meas. Tech. Discuss., doi:10.5194/amt-2017-65, 2017
Manuscript under review for journal Atmos. Meas. Tech.
Discussion started: 18 April 2017

Atmospheric Measurement Techniques Discussions

The scattering coefficient β_{sca} at 450, 550, and 700 nm measured by the nephelometer between 7 and 170° was corrected for the size-dependent angular truncation of the sensing volume to report it to the full angular range 0°-180° (Anderson and Ogren, 1998). Two different approaches were used: for sub-micrometric ammonium sulfate, the correction proposed by Anderson and Ogren (1998) was applied, while for aerosols with a significant coarse fraction (dust, ambient air and kaolinite), the truncation correction was estimated by optical calculations according to the Mie theory for homogeneous spherical particles using as input the measured number size distribution. In the calculations the real and the imaginary parts of the complex refractive index m (m=n-*i*k, where n is the real part and k is the imaginary part) were varied in the wide range 1.42–1.56 and 0.001–0.025*i* for dust (Di Biagio et al., 2017), and 1.50–1.72 and 0.001–0.1*i* for ambient air (Di Biagio et al., 2016), while the value of 1.56-0.001*i* was assumed for kaolinite (Egan and Hilgeman, 1979; Utry et al., 2015). Then, n and k were set to the values which reproduced the measured β_{sca} at 7-170°. The truncation correction factor (C_{trunc}) was estimated as the ratio of the modelled β_{sca} at 0°-180° and 7°-170°. At the three nephelometer wavelengths (450, 550, and 700 nm) the correction factor C_{trunc} varied in the range 1.03-1.06 for ammonium sulfate, 1.08-1.6 for dust, 1.03-1.05 for kaolinite, and 1.05-1.25 for ambient air. Once corrected for truncation, the spectral β_{sca} was used to calculate the scattering Ångström exponent (α_S), applied then to extrapolate β_{sca} at 630 and 660 nm.

3.4.3. Determination of the single scattering albedo (SSA)

The aerosol single scattering albedo (SSA) represents the ratio of scattering to extinction. At 450 nm, the SSA was estimated by nephelometer and CAPS data (Eq. 10), while at 660 nm CAPS data were combined with MAAP observations (Eq. 11):

$$SSA(450)=\frac{\beta_{sca}(450)_{nephelometer}}{\beta_{ext}(450)_{CAPS}} \quad (10)$$

$$SSA(660)=\frac{\beta_{ext}(660)_{CAPS}-\beta_{abs-MAAP}(660)}{\beta_{ext}(660)_{CAPS}} \quad (11)$$

3.5. Number size distribution and effective fine and coarse diameter

The number size distribution was measured by a combination of SMPS and OPC observations. For the SMPS, corrections for particle loss by diffusion in the instrument tubing and the contribution of multiple-charged particles were performed using the SMPS software. The electrical mobility diameter measured by the SMPS can be converted to a geometrical diameter (D_g) by taking into account the particle dynamic shape factor (χ; $D_g=D_m/\chi$). In this study, the SMPS showed a good agreement with OPC data for a shape factor χ=1, which corresponds to spherical particles.

The OPC optical-equivalent nominal diameters were converted into sphere-equivalent geometrical diameters (D_g) by taking into account the aerosol complex refractive index. For dust aerosols the refractive index was varied in the range 1.47-1.53 (n) and 0.001-0.005*i* (k) and D_g was set at the mean ± one standard deviation of the values obtained for the different n and k. For kaolinite the OPC diameter conversion was performed by setting the refractive index at 1.56-0.001*i*. For ambient air the

Atmos. Meas. Tech. Discuss., doi:10.5194/amt-2017-65, 2017
Manuscript under review for journal Atmos. Meas. Tech.
Discussion started: 18 April 2017

Atmospheric Measurement Techniques Discussions

refractive index was set at 1.60-0.01*i*, a value that represents a medium absorbing urban polluted aerosol (see Di Biagio et al., 2016). After conversion, the OPC diameter range became 0.28-18.0 μm for dust (taking into account the particle cut at ~20 μm due to the use of the impactor), and 0.27-58.0 μm for kaolinite and 0.28-65.1 μm for ambient air (the impactor was not used in these cases). The uncertainty was <15% at all diameters.

The aerosol effective fine ($D_{eff,fine}$) and coarse ($D_{eff,coarse}$) diameter were estimated from OPC data as

$$D_{eff,fine} = \frac{\int_{0.3\mu m}^{1.0\mu m} D_g^3 \frac{dN}{dlogD_g} dlogD_g}{\int_{0.3\mu m}^{1.0\mu m} D_g^2 \frac{dN}{dlogD_g} dlogD_g} \quad (12)$$

$$D_{eff,coarse} = \frac{\int_{1\mu m}^{10\mu m} D_g^3 \frac{dN}{dlogD_g} dlogD_g}{\int_{1\mu m}^{10\mu m} D_g^2 \frac{dN}{dlogD_g} dlogD_g} \quad 13)$$

3.6. Data integration and error analysis

Aethalometer data were first processed at 2-min resolution to obtain the time evolution of the attenuation coefficients β_{ATT} and β_{ATT}/R. Data from the MAAP, CAPS, nephelometer, OPC and SMPS were averaged over 2-min to report them to the same resolution of the aethalometer.

Then the β_{ATT} and β_{ATT}/R were calculated over the whole duration of each experiment from Eq. (1) and (6). Corresponding averages of the reference absorption coefficient ($\beta_{abs\text{-}ref}$) were calculated for each experiment and used to estimate C_{ref}. Experiment-averages of SSA, $D_{eff,fine}$, and $D_{eff,coarse}$ were also calculated to relate to the obtained C_{ref}.

The uncertainty on C_{ref} was estimated with the error propagation formula by taking into account the uncertainties on β_{ATT}, β_{ATT}/R, and the standard deviation of the averaged $\beta_{abs\text{-}ref}$ from the CAPS-nephelometer and the MAAP. The uncertainty on β_{ATT} was estimated as the quadratic combination of the uncertainty on the linear fit of ΔATT with respect to time and the uncertainties on the surface deposit A. The uncertainty on β_{ATT}/R was estimated taking into account the uncertainty on β_{ATT} and R. Uncertainties on β_{ATT} and β_{ATT}/R are both ~20%.

4. Results

The time series of observations for all the experiments are shown in **Fig. 2** as 2-min averages. Seven experiments were performed on mineral dust issued from six different areas in the Sahel (Niger), Eastern Asia (China), North America (Arizona), Northern Africa (Tunisia), Australia, and Southern Africa (Namibia), and on a kaolinite powder. Experiments were performed between the 3rd and the 9th of November 2016 and lasted between 1 and 2 hours each. The experiment on Niger dust (labelled as Niger 1 and Niger 2) were duplicated to test the repeatability of the obtained C_{ref}. Ambient air data were collected between the 8th and the 14th November 2016 for a total of 7 hours of measurements. Eight different periods characterized by little variation and different levels of SSA were selected in the

whole set of ambient air measurements. These are identified as ambient air 1 to 8. The summary of information is provided in **Table 2**. SMPS data were available for ammonium sulfate and kaolinite experiments, for one of the two Niger dust experiments (Niger 2), and for some of the ambient air experiments. OPC measurements were performed for all experiments with the exception of the ammonium sulfate.

4.1. Quality control data

Results of the ammonium sulfate control experiment (24 October 2016), used to test the performances of the optical instruments, are illustrated in **Fig. 3**. As expected for this purely scattering aerosol (Toon et al., 1976), the nephelometer scattering and the CAPS extinction at 450 and 630 nm were in very good agreement (less than 4% difference) during the whole duration of the experiment. This is further explicated by the scatterplot of their respective 10-minute averages, yielding a linear regression in the form of y=0.95x+5.1 (R^2=0.95) at 450 nm and y=1.01x-1.4 (R^2=0.98) at 630 nm. The average β_{ext} at 450 and 630 nm from CAPS observations was 913 (± 52) and 424 (± 33) Mm^{-1}, respectively, while the average β_{sca} was 921 (± 36) and 420 (± 17). This led to an average SSA of 1.01 (± 0.07) at 450 nm and 0.99 (± 0.07) at 630 nm.

The absorption coefficient, averaged over the duration of the experiment, was 0.10 (± 0.04) Mm^{-1} at 450 nm and 0.24 (± 0.07) Mm^{-1} at 660 nm according to the aethalometer, and 0.82 (± 0.13) Mm^{-1} at 660 nm according to the MAAP. For the aethalometer, the absorption coefficient was calculated from Eq. (2) assuming C_{ref}=2.14 and the R formulation by C2010 (Eq. 6b). The α(λ) coefficient was calculated from Eq. (3). The c and d terms in Eq. (3) were determined from the power-law fit of $\beta_{ATT}(\lambda)$ vs $\beta_{sca}(\lambda)$ and are c=(0.56 ± 0.06) Mm^{-1} and d=(0.485 ± 0.09). These values are lower than those reported by Arnott et al. (2005) (c=0.797, d=0.564). The A and α_S terms, obtained from the power law fit of $\beta_{sca}(\lambda)$ vs wavelength (Eq. 3) are A=(4.07 ± 0.49)10^9 Mm^{-1} and α_S=(-2.46 ± 0.12).

Figure 4 shows the extinction coefficient at 660 nm extrapolated from CAPS observations and calculated as the sum of nephelometer and MAAP data for dust, kaolinite, and ambient air experiments. The linear regression of the data yields y=1.03x-0.5 (R^2=0.99), indicating the consistency of optical measurements between the CAPS, nephelometer, and MAAP (less than 3% difference on average). Based on the success of the optical closure at 660 nm, we therefore assume the "CAPS minus nephelometer" approach appropriate to estimate the aerosol absorption coefficient at 450 nm.

4.2. Estimate of C_{ref}

The C_{ref}^{*}, C_{ref}(W2003) and C_{ref}(C2010) at 450 and 660 nm obtained for all different experiments and the corresponding aerosol SSA, $D_{eff,fine}$, and $D_{eff,coarse}$ are summarized in **Table 2**.

C_{ref} for mineral dust varied between 1.81 and 2.56 for a SSA of 0.85–0.96 at 450 nm and between 1.75 and 2.28 for a SSA of 0.98–0.99 at 660 nm. The estimate for Niger 1 and 2 samples agreed within 4.9%, which suggests a good repeatability of the C_{ref} estimate. For kaolinite C_{ref} was 2.47–2.51 and 2.31–2.34 at 450 and 660 nm, respectively, with an associated SSA of 0.96 and 0.97 at the two wavelengths. For ambient air C_{ref} varied in the range 1.91–4.35 for a SSA of 0.62–0.87 at 450 nm and

Atmos. Meas. Tech. Discuss., doi:10.5194/amt-2017-65, 2017
Manuscript under review for journal Atmos. Meas. Tech.
Discussion started: 18 April 2017

Atmospheric Measurement Techniques Discussions

1.66–2.96 for and SSA of 0.42–0.76 at 660 nm. For samples 6 and 8 the C_{ref} at 450 was lower than at 660 nm. Otherwise, for all other cases, the C_{ref} was larger at 450 nm than at 660 nm.

Differences within 2.8% were obtained between C_{ref}^{*}, C_{ref}(W2003) and C_{ref}(C2010) at 450 and 660 nm for weakly-absorbing dust and kaolinite. Instead, for more absorbing ambient air aerosols the differences between C_{ref}^{*}, C_{ref}(W2003) and C_{ref}(C2010) were in the range 2.7% to 24.3%. In some cases (ambient air 1–2 and Niger 1 samples) we obtained C_{ref}(C2010)>C_{ref}(W2003); these cases correspond to a mean aethalometer measured ATT<10%, for which R(W2003)>R(C2010), and this explains the larger C_{ref}(C2010). Conversely, C_{ref}(C2010)<C_{ref}(W2003) when the measured ATT was ~15-20%, yielding R(W2003)<R(C2010). The percent difference between the obtained C_{ref}(W2003) and C_{ref}(C2010) increased for decreasing SSA due to the increase of the R(W2003) to R(C2010) absolute difference for decreasing SSA. When averaging data for all ambient air samples, the two formulations yield very similar values. For example, at 660 nm the mean C_{ref}(W2003) was 2.44 (± 0.38), less than 2% larger than the mean C_{ref}(C2010) of 2.39 (± 0.35).

The different ATT threshold assumed here (20%) compared to W2003 and C2010 (10%) has a negligible impact (less than 1% difference) on the results.

The mean and standard deviation of the multiple scattering correction at 450 and 660 nm for dust, kaolinite, and ambient air calculated as the mean of the C_{ref}^{*}, C_{ref}(W2003), and C_{ref}(C2010) is reported in **Table 3**. The mean C_{ref} at 450 and 660 nm is 2.09 (± 0.22) and 1.92 (± 0.17) for dust, 2.49 (± 0.02) and 2.32 (± 0.01) for kaolinite, and 2.32 (± 0.36) and 2.32 (± 0.35) for pollution aerosols

4.3. Dependence of C_{ref} on SSA

As reported in Table 2, very different SSA values at 450 and 660 nm were obtained for the various cases. For dust aerosols, the measured SSA values were larger than 0.85 at 450 nm and close to unity (>0.98) at 660 nm, in line with field observations of dust from different sources (Schladitz et al., 2009; Formenti et al., 2011; Ryder et al., 2013). The SSA for kaolinite was 0.96–0.97 at 450 and 660 nm, in agreement with Utry et al. (2016) (0.97 and 0.99 (±0.04) at 450 and 635 nm, respectively). Both at 450 and 660 nm, the single scattering albedo for ambient air varied in the wide range 0.2 to 0.9 during the whole measurement period (see Fig. 2 for measurements at 660 nm). The average values obtained for air samples 1–8 were 0.62–0.87 at 450 and 0.42–0.76 at 660 nm. The SSA decreased with increasing wavelength, as expected for pollution aerosols (e.g., Bergstrom et al., 2007; Di Biagio et al., 2016). The wide range of values indicates the occurrence of particles with very different absorption properties, henceforth chemical composition. For instance, in urban environments, Bergstrom et al. (2007) reported SSA in the range 0.2–1.0 at 550 nm, with lowest values observed for soot-dominated air masses and highest values for urban pollution dominated by low-absorbing organic components.

The experimental SSA values served to two purposes. First, as shown in **Fig. 5**, they are linearly related to the factor f in the shadowing effect correction term R in Eq. (6a)-(6b) as f=a(1-SSA)+1. The linear regression of our data yields a slope a=(1.48 ± 0.14), larger than the value of 0.85 reported in W2003 (f data from W2003 are also shown in Fig. 5) and 0.76 in C2010.

Secondly, SSA data serve to investigate the dependence of C_{ref} on particle absorption for mineral dust. As shown in **Fig. 6** (top panel), C_{ref} for dust seems to be independent of SSA at 660 nm, whereas it decreases for increasing SSA at 450 nm. This trend is statistically significant (correlation coefficient of R^2=0.85). The relationship between C_{ref} and SSA is also investigated in **Fig. 6** (bottom panel) for all aerosol samples. Globally, Fig. 6 suggests a decrease of C_{ref} for increasing SSA, in particular at 450 nm, albeit with a poorer statistical significance at both wavelengths (R^2=0.35 and 0.59). Data are also compared to those reported in W2003 and C2010 at 660 nm for different aerosol types. Diesel soot and soot mixed with ammonium sulfate were investigated in W2003, while C2010 reported data for ambient aerosols sampled at different locations in Europe and in Amazonia. W2003 also reported the C_{ref} for soot particles at 450 nm (not shown in Fig. 6), with values between 2.08 and 3.64; these values are in line with our observations at 450 nm for ambient air. Whereas, as illustrated in Fig. 6, both W2003 and C2010 found a relationship between C_{ref} and SSA at 660 nm, contrasting results are obtained when plotting the two datasets together. C2010 obtained a sharp and almost linear decrease of C_{ref} with increasing SSA (C_{ref}~5–2.5 for SSA~0.65–0.9), while W2003 data showed a pronounced decrease of C_{ref} (~2–4) for increasing SSA in the range 0.5 and 0.7 and low C_{ref} values (~2) at SSA~0.2. Our data for dust and kaolinite at high SSA (>0.97) seem to follow the same linear relationship as C2010. However at lower SSA, our data for ambient aerosols are closer to W2003 results at 660 nm. These differences between W2003 and C2010 data, and also with our results, are quite difficult to explain. The main difference between W2003 compared to C2010 is that W2003 performed measurements in a simulation chamber, while C2010 was a field study. Working in ambient conditions may influence the retrieved C_{ref}. In fact, volatile-organic compounds or water vapor present in the atmosphere may condense on the filter, thus enhancing the scattering from the filter fibers and leading to higher C_{ref}. This could explain the higher C_{ref} obtained in C2010 compared to W2003. Our results for ambient air particles, however, are in agreement with W2003 chamber results. Differences in the size distributions of the investigated aerosols are also expected to possibly affect the comparison; however, no detailed information on the size of investigated aerosols is provided in W2003 and C2010. Another source of discrepancy may be in the fact that, differently from W2003 and our study, where aethalometer and MAAP were compared at 660 nm, C_{ref} in C2010 was estimated by comparing aethalometer data at 660 nm with MAAP observations at 630 nm. As aerosol absorption increases with decreasing wavelength, this wavelength difference may induce an underestimation of C_{ref} in C2010.

4.4. Dependence of C_{ref} on particles size

Examples of the number size distribution measured by the SMPS and OPC for ammonium sulfate, Niger dust, kaolinite, and ambient air are shown in **Fig. 7**. Ammonium sulfate had mostly a submicron distribution, while dust aerosols presented the largest fraction over the whole super-micron range up to about 10-20 µm. Dust particles larger than 20 µm were completely suppressed by the impactor system and were not detected by the OPC. The coarse component, up to about 10 µm, was also identified in the kaolinite and ambient air samples. In particular, a defined mode at ~4 µm was detected in ambient air particles, may be linked to the presence of soot-aggregates, tire abrasions, re-suspended road dust, or bioaerosols (Harrison et al., 2001; Bauer et al., 2008; Pakbin et al., 2010; Liu

and Harrison, 2011). In correspondence, the $D_{eff,fine}$ varied between 0.24 and 0.62 μm and the $D_{eff,coarse}$ between 2.3 and 6.2 μm for the different cases (Table 2). For mineral dust, $D_{eff,coarse}$ ranged between 2.3 and 3.6 μm, encompassing the value of $D_{eff,coarse}$ ~ 3 μm reported by Denjean et al. (2016b) in their figure 11 for Saharan dust both close to sources and during transport over the Atlantic.

These observations are consistent with the extinction (α_E) and the absorption (α_A) Ángstrom exponent measured during the experiments. The α_E (shown in Fig.3) was ~1 for kaolinite, varied between about 1 and 2 for mineral dust aerosols, and between 0.5 and 2.5 for ambient air, indicating particles with variable sizes, both the sub-micron and the super-micron fractions. The absorption Ángström coefficient α_A obtained from aethalometer data was between 2.2 and 3 for dust, and about 1 for kaolinite and ambient air aerosols.

The dependence of C_{ref} at 450 and 660 nm on the effective diameter fine $D_{eff,fine}$ and coarse $D_{eff,coarse}$ as a measure of particle size was investigated. The scatterplot of C_{ref} versus $D_{eff,coarse}$ is shown in **Fig. 8** and indicates that the C_{ref} does not have any statistically significant dependence on the particle size for mineral dust at both wavelengths and for all data at 660 nm ($R^2 \leq 0.40$). Conversely, a slight increase of C_{ref} for increasing $D_{eff,coarse}$ is obtained at 450 nm when all aerosol samples are considered ($R^2=0.70$). No dependence of C_{ref} versus $D_{eff,fine}$ is instead obtained for all cases ($R^2 \leq 0.44$) (not shown).

5. Conclusions

In this paper we presented an intercomparison study between an aethalometer and a MAAP, a nephelometer, and two CAPS with the aim of determining a two-wavelength multiple scattering correction (C_{ref}) for aethalometer measurements for weakly-absorbing mineral dust aerosols. Mineral dust aerosols investigated here were generated from natural parent soils collected in desert areas, both in the Northern and in the Southern hemisphere (Di Biagio et al., 2014; 2017). The size distribution of the generated dust included both the submicron and the supermicron fractions, with an effective fine and coarse diameter between 0.32–0.55 and 2.3–3.6 μm, respectively.

The estimated C_{ref} was in the range 1.81–2.56 at 450 nm and 1.75–2.28 at 660 nm for the different dust samples, with mean C_{ref} values of 2.09 (± 0.22) and 1.92 (± 0.17), respectively. The dust absorption coefficient estimated by the aethalometer should henceforth be about 2% (450 nm) and 11% (660 nm) higher than obtained by using the wavelength-independent value of 2.14, commonly used in the literature (e.g., Sandradewi et al., 2008; Formenti et al., 2011; Di Biagio 2016). The new estimate of C_{ref} has a negligible impact on the dust SSA at 450 nm (less than 0.5% difference between the value obtained for C_{ref}=2.09 or 2.14), but affects by up to ~3% the estimate of SSA at 660 nm.

Given that the maximum intensity of the solar spectrum occurs at about 700 nm, the expected change in the dust SSA at 660 nm may significantly affect the impact of dust on radiation. Mallet et al. (2009) estimated that about a 3% change in the visible SSA of dust may determine up to a 10% change in

the radiative effect of dust at the surface, and up to 20% change at the Top of the Atmosphere, with a net ~25% increase of dust absorption in the atmosphere. Given the strong sensitivity of the dust direct effect to particle absorption (Solmon et al., 2008; Mallet et al., 2009; Di Biagio et al., 2010; Jin et al., 2016, among others), we recommend this new C_{ref} value at 660 nm to be used when analyzing aethalometer data for mineral dust aerosols.

The analysis performed in this study indicates that there is no dependence of C_{ref} on the coarse component of the particle size distribution for dust. This suggests that the C_{ref} obtained here can be used to correct aethalometer data for dust at emission, when the coarse fraction dominates the dust size distribution, as well as after long-range transport, when the coarsest component of dust has preferentially settled out.

Finally, even if beyond the scope of the paper, our body of observations, spanning a wide range of SSA values from 0.96–0.97 (kaolinite) to ~0.4–0.8 (ambient urban aerosols), indicates that C_{ref} decreases for increasing SSA, both at 450 and 660 nm. This is generally consistent with the results of W2003 and C2010 at 660 nm. However, a unique relationship cannot be established. At high SSA (>0.90), our data, as well as those of C2010, suggest a sharper decrease than at SSA in the range 0.4-0.8, where our data are more consistent with those of W2003. Differences in aerosol sampling conditions and in the exact analysed wavelengths from the three studies may be the cause of such discrepancy, but clear conclusions, as well as an explicit relationship between C_{ref} and SSA, are still difficult to give. Similarly, our observations seem to indicate that C_{ref} increases for increasing $D_{eff,coarse}$ at 450 nm. This trend was however observed only when the whole aerosol dataset was considered, and not if we limited to dust observations, so making difficult to draw clear conclusions.

A more extensive characterization of C_{ref} should be required to provide an appropriate correction of aethalometer data under the wide range of atmospheric conditions.

Author contributions

C. Di Biagio and P. Formenti designed the experiments, discussed the results, and wrote the manuscript with comments from all co-authors. N. Marchand provided the MAAP used in the experiments. C. Di Biagio, M. Cazaunau, and E. Pangui performed the experiments. C. Di Biagio performed the data analysis.

Acknowledgements

The RED-DUST project was supported by the French national programme LEFE/INSU, by the Institut Pierre Simon Laplace (IPSL), and by OSU-EFLUVE (Observatoire des Sciences de l'Univers-Enveloppes Fluides de la Ville à l'Exobiologie) through dedicated research funding. C. Di Biagio was supported by the CNRS via the Labex L-IPSL, which is funded by the ANR (grant no. ANR-10-LABX-0018). This work has also received funding from the European Union's Horizon 2020 (H2020) research and innovation programme through the EUROCHAMP-2020 Infrastructure Activity under

grant agreement No 730997. The authors thank K. Kandler, D. Seibert, and the LISA staff who collected the soil samples used in this study, E. Journet who provided the kaolinite sample, A. Petzold for helpful discussions on the aethalometer multiple scattering effects, and B. Tamime-Roussel for logistic help with the MAAP.

References

Anderson, T. L. and Ogren, J. A.: Determining aerosol radiative properties using the TSI 3563 integrating nephelometer, Aerosol Sci. Technol., 29, 57–69, 1998.

Andreae, M. O. and Gelencsér, A.: Black Carbon or Brown Carbon? The Nature of Light-Absorbing Carbonaceous Aerosols. Atmos. Chem. Phys. 6:3131–3148, 2006.

Arnott, W. P., Hamasha, K., Moosmüuller, H., Sheridan, P. J., and Ogren, J. A.: Towards aerosol light-absorption measurements with a 7-wavelength aethalometer: Evaluation with a photoacoustic instrument and 3-wavelength nephelometer, Aerosol Sci. Tech., 39, 17–29, 2005.

Backman, J., Schmeisser, L., Virkkula, A., Ogren, J. A., Asmi, E., Starkweather, S., Sharma, S., Eleftheriadis, K., Uttal, T., Jefferson, A., Bergin, M., and Makshtas, A.: On Aethalometer measurement uncertainties and multiple scattering enhancement in the Arctic, Atmos. Meas. Tech. Discuss., doi:10.5194/amt-2016-294, in review, 2016.

Balkanski, Y., Schulz, M., Claquin, T., and Guibert, S.: Reevaluation of Mineral aerosol radiative forcings suggests a better agreement with satellite and AERONET data, Atmos. Chem. Phys., 7, 81–95, doi:10.5194/acp-7-81-2007, 2007.

Bauer, H., Schueller, E., Weinke, G., Berger, A., Hitzenberger, R., Marr, I. L., and Puxbaum, H.: Significant contributions of fungal spores to the organic carbon and to the aerosol mass balance of the urban atmospheric aerosol, Atmos. Environ., 42, 5542-5549, 2008.

Bergstrom, R. W., Pilewskie, P., Russell, P. B., Redemann, J., Bond, T. C., Quinn, P. K., and Sierau, B.: Spectral absorption properties of atmospheric aerosols, Atmos. Chem. Phys., 7, 5937-5943, doi:10.5194/acp-7-5937-2007, 2007.

Bond, T. C., Anderson, T. L., and Campbell, D.: Calibration and intercomparison of filter-based measurements of visible light absorption by aerosols, Aerosol Sci. Tech., 30(6), 582–600, 1999.

Boucher, O., Randall, D., Artaxo, P., Bretherton, C., Feingold, G., Forster, P., Kerminen, V.-M., Kondo, Y., Liao, H., Lohmann, U., Rasch, P., Satheesh, S. K., Sherwood, S., Stevens, B., and Zhang, X. Y.: Clouds and Aerosols. In: Climate Change 2013: The Physical Science Basis. Contribution of Working Group I to the Fifth Assessment Report of the Intergovernmental Panel on Climate Change [Stocker, T.F., D. Qin, G.-K. Plattner, M. Tignor, S.K. Allen, J. Boschung, A. Nauels, Y. Xia, V. Bex and P.M. Midgley (eds.)]. Cambridge University Press, Cambridge, United Kingdom and New York, NY, USA, 2013.

Caponi, L., Formenti, P., Massabó, D., Di Biagio, C., Cazaunau, M., Pangui, E., Chavailler, S., Landrot, G., Fonda, E., Andreae', M. O., Kandler, K., Piketh, S., Saeed, T., Seibert, D., Williams, E., Balkanski, Y., Prati, P., and Doussin, J.-F.: Spectral- and size-resolved shortwave mass absorption cross-sections of mineral dust aerosols: a smog chamber study, *Atmos. Chem. Phys. Discuss.*, doi:10.5194/acp-2017-5, in review, 2017.

Cattrall, C., Carder, K. L., and Gordon, H. R.: Columnar aerosol single-scattering albedo and phase function retrieved from sky radiance over the ocean: measurements of Saharan dust, J. Geophys. Res., 108(D9), 4287, doi:10.1029/2002JD002497, 2003.

Collaud Coen, M., Weingartner, E., Apituley, A., Ceburnis, D., Fierz-Schmidhauser, R., Flentje, H., Henzing, J. S., Jennings, S. G., Moerman, M., Petzold, A., Schmid, O., and Baltensperger, U.: Minimizing light absorption measurement artifacts of the Aethalometer: evaluation of five correction algorithms, Atmos. Meas. Tech., 3, 457–474, doi:10.5194/amt-3-457-2010, 2010.

548 DeCarlo, P., Worsnop, D. R., Slowik, J. G., Davidovits, P., and Jimenez, J. L.: Particle Morphology
549 and Density Characterization by Combined Mobility and Aerodynamic Diameter Measurements. Part
550 1: Theory, Aerosol Sci. Technol., 38(12), 1185-1205, 2004.

551 Denjean, C., Formenti, P., Desboeufs, K., Chevaillier, S., Triquet, S., Maillé, M., Cazaunau, M.,
552 Laurent, B., Mayol-Bracero, O. L., Vallejo, P., Quiñones, M., Gutierrez-Molina, I. E., Cassola, F.,
553 Prati, P., Andrews, E., and Ogren, J.: Size distribution and optical properties of African mineral dust
554 after intercontinental transport, J. Geophys. Res. Atmos., 121, 7117–7138,
555 doi:10.1002/2016JD024783, 2016a.

556 Denjean, C., Cassola, F., Mazzino, A., Triquet, S., Chevaillier, S., Grand, N., Bourrianne, T.,
557 Momboisse, G., Sellegri, K., Schwarzenbock, A., Freney, E., Mallet, M., and Formenti, P.: Size
558 distribution and optical properties of mineral dust aerosols transported in the western Mediterranean,
559 Atmos. Chem. Phys., 16, 1081-1104, doi:10.5194/acp-16-1081-2016, 2016b.

560 Di Biagio, C., di Sarra, A., and Meloni, D.: Large atmospheric shortwave radiative forcing by
561 Mediterranean aerosols derived from simultaneous ground-based and spaceborne observations and
562 dependence on the aerosol type and single scattering albedo, J. Geophys. Res., 115, D10209, doi:
563 10.1029/2009JD012697, 2010.

564 Di Biagio, C., Formenti, P., Styler, S. A., Pangui, E., and Doussin, J.-F.: Laboratory chamber
565 measurements of the longwave extinction spectra and complex refractive indices of African and
566 Asian mineral dusts, Geophys. Res. Lett., 41, 6289-6297, doi:10.1002/2014GL060213, 2014.

567 Di Biagio, C., Formenti, P., Doppler, L., Gaimoz, C., Grand, N., Ancellet, G., Attié, J.-L., Bucci, S.,
568 Dubuisson, P., Fierli, F., Mallet, M., and Ravetta, F.: Continental pollution in the Western
569 Mediterranean basin: large variability of the aerosol single scattering albedo and influence on the
570 direct shortwave radiative effect, Atmos. Chem. Phys., 16, 10591-10607, doi:10.5194/acp-16-10591-
571 2016, 2016.

572 Di Biagio, C., Formenti, P., Balkanski, Y., Caponi, L., Cazaunau, M., Pangui, E., Journet, E., Nowak,
573 S., Caquineau, S., Andreae', M. O., Kandler, K., Saeed, T., Piketh, S., Seibert, D., Williams, E., and
574 Doussin, J.-F.: Global scale variability of the mineral dust longwave refractive index: a new dataset
575 of in situ measurements for climate modelling and remote sensing, Atmos. Chem. Phys., 17, 1901-
576 1929, doi:10.5194/acp-17-1901-2017, 2017.

577 di Sarra, A., C. Di Biagio, D. Meloni, F. Monteleone, G. Pace, S. Pugnaghi, and D. Sferlazzo,
578 Shortwave and longwave radiative effects of the intense Saharan dust event of March 25-26, 2010,
579 at Lampedusa (Mediterranean sea), J. Geophys. Res., 116, D23209, doi:10.1029/2011JD016238,
580 2011.

581 Egan, W. G. and Hilgeman, T. W.: Optical Properties of Inhomogeneous Materials: Applications to
582 Geology, Astronomy, Chemistry, and Engineering, Academic Press, 235 pp, 1979.

583 Fialho, P., Hansenb, A. D. A., and Honrath, R. E.: Absorption coefficients by aerosols in remote
584 areas: a new approach to decouple dust and black carbon absorption coefficients using seven-
585 wavelength Aethalometer data, Aerosol Sci., 36, 267–282, 2005.

586 Formenti, P., Rajot, J. L., Desboeufs, K., Said, F., Grand, N., Chevaillier, S., and Schmechtig, C.:
587 Airborne observations of mineral dust over western Africa in the summer Monsoon season: spatial
588 and vertical variability of physico-chemical and optical properties, Atmos. Chem. Phys., 11, 6387-
589 6410, doi:10.5194/acp-11-6387-2011, 2011.

590 Ginoux, P., Prospero, J. M., Gill, T. E., Hsu, N. C., and Zhao, M.: Global-scale attribution of
591 anthropogenic and natural dust sources and their emission rates based on MODIS Deep Blue
592 aerosol products, Rev. Geophys., 50, RG3005, doi:10.1029/2012RG000388, 2012.

593 Goudie A. S., and Middleton, N. J.: Desert dust in the global system. Springer, Berlin, Heidelberg,
594 New York, 2006.

595 Hansen, A. D. A., Rosen, H., and Novakov, T.: The aethalometer—an instrument for the real-time
596 measurement of optical absorption by aerosol particles. The Science of the Total Environment, 36,
597 191–196, 1984.

598 Harrison, R. M., Yin, J., Mark, D., Stedman, J., Appleby, R.S., Booker, J., and Moorcroft, S.: Studies
599 of the coarse particle (2.5–10 μm) component in UK urban atmospheres, Atmos. Environ., 35,
600 3667–3679, 2001.

601 Heim, M., Mullins, B. J., Umhauer, H., and Kasper, G.: Performance evaluation of three optical
602 particle counters with an efficient “multimodal” calibration method, J. Aerosol Sci., 39, 1019–1031,
603 2008.

604 Heinold, B., I. Tegen, K. Schepanski, and O. Hellmuth, Dust radiative feedback on Saharan boundary
605 layer dynamics and dust mobilization, Geophys. Res. Lett., 35, L20817,
606 doi:10.1029/2008GL035319, 2008.

607 Jin, Q., Zang, Z.-L., and Wei, J.: High sensitivity of Indian summer monsoon to Middle East dust
608 absorptive properties, Sci. Rep, 6:30690, doi: 10.1038/srep30690, 2016.

609 Kandler, K., Schütz, L., Deutscher, C., Ebert, M., Hofmann, H., Jäckel, S., Jaenicke, R., Knippertz, P.,
610 Lieke, K., Massling, A., Petzold, A., Schladitz, A.,Weinzierl, B.,Wiedensohler, A., Zorn, S., and
611 Weinbruch, S.: Size distribution, mass concentration, chemical and mineralogical composition and
612 derived optical parameters of the boundary layer aerosol at Tinfou, Morocco, during SAMUM 2006,
613 Tellus B, 61, 32–50, doi:10.1111/j.1600-0889.2008.00385.x, 2009.

614 Knippertz, P., and Stuut, J.-B. W.: Mineral Dust: A Key Player in the Earth System, Eds. Springer,
615 327-357, doi:10.1007/978-94-017-8978-3_13, 2014.

616 Liu, X. J., and Harrison, R. M.: Properties of coarse particles in the atmosphere of the United
617 Kingdom, Atmos. Environ., 45, 3267–3276, 2011.

618 Loeb, N. G., and Su, W. Y.: Direct aerosol radiative forcing uncertainty based on a radiative
619 perturbation analysis, J. Clim., 23, 5288–5293, 2010.

620 Mallet, M., Tulet, P., Serça, D., Solmon, F., Dubovik, O., Pelon, J., Pont, V., and Thouron, O.: Impact
621 of dust aerosols on the radiative budget, surface heat fluxes, heating rate profiles and convective
622 activity over West Africa during March 2006, Atmos. Chem. Phys., 9, 7143-7160, doi:10.5194/acp-9-
623 7143-2009, 2009.

624 Massoli, P., Kebabian, P. L., Onasch, T. B., Hills, F. B., and Freedman, A.: Aerosol Light Extinction
625 Measurements by Cavity Attenuated Phase Shift (CAPS) Spectroscopy: Laboratory Validation and
626 Field Deployment of a Compact Aerosol Particle Extinction Monitor, Aerosol Sci. Technol., 44, 428–
627 435, doi:10.1080/02786821003716599, 2010.

628 Miller, R.L., I. Tegen, and J.P. Perlwitz: Surface radiative forcing by soil dust aerosols and the
629 hydrologic cycle. J. Geophys. Res., 109, D04203, doi:10.1029/2003JD004085, 2004.

630 Müller, T., Henzing, J. S., de Leeuw, G., Wiedensohler, A., Alastuey, A., Angelov, H., Bizjak, M.,
631 Collaud Coen, M., Engström, J. E., Gruening, C., Hillamo, R., Hoffer, A., Imre, K., Ivanow, P.,
632 Jennings, G., Sun, J. Y., Kalivitis, N., Karlsson, H., Komppula, M., Laj, P., Li, S.-M., Lunder, C.,
633 Marinoni, A., Martins dos Santos, S., Moerman, M., Nowak, A., Ogren, J. A., Petzold, A., Pichon, J.
634 M., Rodriquez, S., Sharma, S., Sheridan, P. J., Teinilä, K., Tuch, T., Viana, M., Virkkula, A.,
635 Weingartner, E., Wilhelm, R., and Wang, Y. Q.: Characterization and intercomparison of aerosol
636 absorption photometers: result of two intercomparison workshops, Atmos. Meas. Tech., 4, 245-268,
637 doi:10.5194/amt-4-245-2011, 2011.

638 Pakbin, P., Hudda, N., Cheng, K. L., Moore, K. F., Sioutas, C.: Spatial and temporal variability of
639 coarse ($PM_{10–2.5}$) particulate matter concentrations in the Los Angeles area, Aerosol Sci. Technol.,
640 44, 514–525, 2010.

641 Perez, C., Nickovic, S., Baldasano, J. M., Sicard, M., Rocadenbosch, F., and Cachorro, V. E.: A long
642 Saharan dust event over the western Mediterranean: Lidar, Sun photometer observations, and
643 regional dust modeling, J. Geophys. Res., 111, D15214, doi:10.1029/2005JD006579, 2006.

644 Petzold, A., and Schönlinner, M.: MultiangleAbsorption Photometry–A New Method for the
645 Measurement of Aerosol Light Absorption and Atmospheric Black Carbon, J. Aerosol Sci., 35:421–
646 441, 2004.

647 Petzold, A., Schloesser, H., Sheridan, P. J., Arnott, W. P., Ogren, J. A., and Virkkula, A.: Evaluation of
648 Multi-angle Absorption Photometry for Measuring Aerosol Light Absorption, Aerosol Sci. Technol.,
649 39, 40–51, 2005.

650 Querol, X., Pey, J., Pandolfi, M., Alastuey, A., Cusack, M., Pérez, N., Moreno, T., Viana, M.,
651 Mihalopoulos, N., Kallos, G., and Kleanthous, S.: African dust contributions to mean ambient PM10
652 mass-levels across the Mediterranean Basin, Atmos. Environ., 43, 4266-4277, 2009.

653 Ramana, M. V., and Ramanathan, V.: Abrupt transition from natural to anthropogenic aerosol
654 radiative forcing: Observation at the ABCMaldives Climate Observatory, J. Geophys. Res., 111,
655 D20207, doi:10.1029/2006JD007063, 2006.

656 Reddy, M. S., O. Boucher, Y. Balkanski, and M. Schulz, Aerosol optical depths and direct radiative
657 perturbations by species and source type. Geophys. Res. Lett., 32, L12803, 2005.

658 Redmond, H. E., Dial, K. D., and Thompson, J. E.: Light scattering and absorption by wind blown
659 dust: Theory, measurement, and recent data, Aeolian Res., 2, 5–26, 2010.

660 Ryder, C. L., Highwood, E. J., Rosenberg, P. D., Trembath, J., Brooke, J. K., Bart, M., Dean, A.,
661 Crosier, J., Dorsey, J., Brindley, H., Banks, J., Marsham, J. H., McQuaid, J. B., Sodemann, H., and
662 Washington, R.: Optical properties of Saharan dust aerosol and contribution from the coarse mode
663 as measured during the Fennec 2011 aircraft campaign, Atmos. Chem. Phys., 13, 303-325,
664 doi:10.5194/acp-13-303-2013, 2013.

665 Sandradewi, J., Prévôt, A. S. H., Weingartner, E., Schmidhauser, R., Gysel, M., and Baltensperger,
666 U.: A study of wood burning and traffic aerosols in an Alpine valley using a multi-wavelength
667 Aethalometer, Atmos. Environ., 42, 101-112, 2008.

668 Saturno, J., Pöhlker, C., Massabò, D., Brito, J., Carbone, S., Cheng, Y., Chi, X., Ditas, F., Hrabě de
669 Angelis, I., Morán-Zuloaga, D., Pöhlker, M. L., Rizzo, L. V., Walter, D., Wang, Q., Artaxo, P., Prati,
670 P., and Andreae, M. O.: Comparison of different Aethalometer correction schemes and a reference
671 multi-wavelength absorption technique for ambient aerosol data, Atmos. Meas. Tech. Discuss.,
672 doi:10.5194/amt-2016-361, in review, 2016.

673 Schladitz, A., Müller, T., Kaaden, N., Massling, A., Kandler, K., Ebert, M., Weinbruch, S., Deutscher,
674 C., and Wiedensohler, A.: In situ measurements of optical properties at Tinfou (Morocco) during the
675 Saharan Mineral Dust Experiment SAMUM 2006, Tellus B, 61, 64–78, doi:10.1111/j.1600-
676 0889.2008.00397.x, 2009.

677 Schmid, O., Artaxo, P., Arnott,W. P., Chand, D., Gatti, L. V., Frank, G. P., Hoffer, A., Schnaiter, M.,
678 and Andreae, M. O.: Spectral light absorption by ambient aerosols influenced by biomass burning in
679 the Amazon Basin. I: Comparison and field calibration of absorption measurement techniques,
680 Atmos. Chem. Phys., 6, 3443–3462, 2006.

681 Segura, S., Estellés, V., Titos, G., Lyamani, H., Utrillas, M. P., Zotter, P., Prévôt, A. S. H., Močnik, G.,
682 Alados-Arboledas, L., and Martínez-Lozano, J. A., Determination and analysis of in situ spectral
683 aerosol optical properties by a multi-instrumental approach, Atmos. Meas. Tech., 7, 2373-2387, doi:
684 10.5194/amt-7-2373-2014, 2014.

685 Slingo, A., et al., Observations of the impact of a major Saharan dust storm on the atmospheric
686 radiation balance, Geophys. Res. Lett., 33, L24817, doi:10.1029/2006GL027869, 2006.

687 Sokolik, I., and Toon, O.: Incorporation of mineralogical composition into models of the radiative
688 properties of mineral aerosol from UV to IR wavelengths, J. Geophys. Res., 104, 9423-9444, 1999.

689 Solmon, F., Mallet, M., Elguindi, N., Giorgi, F., Zakey, A. and Konaré, A.: Dust aerosol impact on
690 regional precipitation over western Africa, mechanisms and sensitivity to absorption properties,
691 Geophys. Res. Lett., 35, L24705, doi:10.1029/2008GL035900, 2008.

692 Toon, O. B., Pollack, J. B., and Khare, B. N.: The Optical Constants of Several Atmospheric Aerosol
693 Species: Ammonium Sulfate, Aluminum Oxide, and Sodium Chloride, J. Geophys. Res., 81, 5733–
694 5748, 1976.

695 Utry, N., Ajtai, T., Pintér, M., Tombácz, E., Illés, E., Bozóki, Z., and Szabó, G.: Mass-specific optical
696 absorption coefficients and imaginary part of the complex refractive indices of mineral dust
697 components measured by a multi-wavelength photoacoustic spectrometer, Atmos. Meas. Tech., 8,
698 401-410, doi:10.5194/amt-8-401-2015, 2015.

699 Virkkula, A., Makela, T., Hillamo, R., Yli-Tuomi, T., Hirsikko, A., Hameri, K., and Koponen, I. K.: A
700 simple procedure for correcting loading effects of aethalometer data, J. Air Waste Manage., 57(10),
701 1214–1222, 2007.

702 von der Weiden, S.-L., Drewnick, F., and Borrmann, S.: Particle Loss Calculator – a new software tool
703 for the assessment of the performance of aerosol inlet systems, Atmos. Meas. Tech., 2, 479–494,
704 2009.

705 Weingartner, E., Saathof, H., Schnaiter, M., Streit, N., Bitnar, B., and Baltensperger, U.: Absorption of
706 light by soot particles: Determination of the absorption coefficient by means of Aethalometers, J.
707 Aerosol Sci., 34, 1445–1463, 2003.

708 Yoshioka, M., N.M.Mahowald, A. J. Conley,W. D. Collins, D.W. Fillmore, C. S. Zender, and D. B.
709 Coleman: Impact of desert dust radiative forcing on sahel precipitation: Relative importance of dust
710 compared to sea surface temperature variations, vegetation changes, and greenhouse gas
711 warming, J. Clim., 20, 1445– 1467, 2007.
712

Table captions

Table 1. Specifications and references of instruments used during experiments.

Table 2. Summary of experiments and results. The mean and the standard deviation of $D_{eff,fine}$, $D_{eff,coarse}$, SSA at 450 and 660 nm, C_{ref}^{*}, C_{ref}(W2003), and C_{ref}(C2010) are reported. As a reminder: C_{ref}^{*} is the multiple scattering correction obtained not taking into account the shadowing effect correction in aethalometer data; C_{ref}(W2003) and C_{ref}(C2010) take the shadowing effect correction into account, by using the parametrisations by Weingartner et al. (2003) (referred as W2003) and Collaud Coen et al. (2010) (referred as C2010), respectively. The maximum of the % difference between C_{ref}^{*}, C_{ref}(W2003), and C_{ref}(C2010) is indicated in the table.

Table 3. Mean and standard deviation multiple scattering correction $\overline{C_{ref}}$ at 450 and 660 nm for dust, kaolinite, and ambient air. The $\overline{C_{ref}}$ was calculated as the mean of the C_{ref}^{*}, C_{ref}(W2003), and C_{ref}(C2010) obtained at each wavelength for the different aerosol types. As a reminder: C_{ref}^{*} is the multiple scattering correction obtained not taking into account the shadowing effect correction in aethalometer data; C_{ref}(W2003) and C_{ref}(C2010) take the shadowing effect correction into account, by using the parametrisations by Weingartner et al. (2003) and Collaud Coen et al. (2010), respectively.

Figure captions

Figure 1. Experimental setup used for the aethalometer intercomparison experiments.

Figure 2. Temporal series of experiments showing the measured optical data at 660 nm. The different panels show (from the top to the bottom): (i) the shadowing-corrected aethalometer attenuation at 660 nm (data corrected with the R formulation by Collaud Coen et al. (2010) (referred as R(C2010)) are shown) and the MAAP aerosol absorption coefficient; (ii) the aerosol extinction at 660 nm extrapolated from CAPS PMex measurements and estimated as the sum of nephelometer scattering and MAAP absorption; (iii) the extinction aerosol Ángstrom exponent; (iv) the aerosol single scattering albedo at 660 nm. Each point in the plot corresponds to 2 min average data. The x-axis indicates the data point sequential number. Experiments with dust samples and kaolinite were realised between the 3rd and the 9th of November 2016 and lasted between 1 and 2 hours each. Ambient air data were collected at different steps between the 8th and the 14th November 2016 for a total of 7 hours of measurements.

Figure 3. Ammonium sulfate experiment. Left panel: temporal evolution of the extinction and scattering coefficients measured by the CAPS PMex and the nephelometer at 450 nm (blue scale) and 630 nm (red scale). Each point in the plot corresponds to 2 min average data. Right panel: CAPS PMex versus nephelometer data (10 minutes averages). The y=x line and the results of the linear fit between CAPS and nephelometer data are also shown in the plot.

Figure 4. CAPS PMex extinction coefficient extrapolated at 660 nm versus nephelometer+MAAP calculated extinction at 660 nm for all experiments (dust, kaolinite, ambient air). Each point in the plot

749 corresponds to 10 min average data. The y=x line and the results of the linear fit between CAPS and
750 nephelometer+MAAP data are also shown in the plot.

751 **Figure 5.** Left panel: estimated f values versus (1-SSA) at 660 nm for dust aerosols. Different
752 symbols are used to distinguish between dust from different sources. Right panel: f versus SSA at
753 660 nm for all experiments. Different symbols are used to distinguish between different aerosol types.
754 The results of the linear fit between f and (1-SSA) are also reported. Data from Weingartner et al.
755 (2003) (W2003) (extracted from their Figure 4) are also shown in the plot for comparison.

756 **Figure 6.** Top panel: C_{ref}(W2003) (multiple scattering correction obtained by taking into account the
757 shadowing effect correction using the parametrisations by Weingartner et al. (2003)) versus SSA at
758 450 and 660 nm for mineral dust samples analysed in this study. Different symbols are used to
759 distinguish between dust from different sources. As indicated in Table 2, the difference between C_{ref}^{*},
760 C_{ref}(W2003), and C_{ref}(C2010) is very low for mineral dust aerosols. Bottom panel: C_{ref} versus SSA at
761 450 and 660 nm for the different aerosol samples analysed in this study. Different symbols are used
762 to distinguish between different aerosol types. Data for both C_{ref}(W2003) and C_{ref}^{*} (multiple scattering
763 correction obtained not taking into account the shadowing effect correction in aethalometer data) are
764 shown for ambient air aerosols, while for dust and kaolinite, for which the difference between the
765 different formulations is very low, only C_{ref}(W2003) is reported. Data from Weigartner et al. (2003)
766 (W2003) (C_{ref} from their Table 3, and SSA extracted from their Fig. 4) and Collaud Coen et al. (2010)
767 (C2010) (extracted from their Fig. 5) at 660 nm are also shown in the plot for comparison. The results
768 of the linear fits between C_{ref} and SSA for mineral dust and for the entire dataset are also shown in the
769 plot.

770 **Figure 7.** Examples of number size distribution (normalised to the total number concentration) for
771 ammonium sulfate, dust (Niger sample), kaolinite, and ambient air aerosols. Data refer to the mean
772 over each experiment as measured from the SMPS and the OPC. Error bars (standard deviations)
773 have been omitted for the sake of clarity.

774 **Figure 8.** Top panel: C_{ref}(W2003) (multiple scattering correction obtained by taking into account the
775 shadowing effect correction using the parametrisations by Weingartner et al. (2003)) at 450 and 660
776 nm versus the effective diameter coarse $D_{eff,coarse}$. for mineral dust samples analysed in this study.
777 Different symbols are used to distinguish between dust from different sources. Bottom panel: C_{ref} at
778 450 and 660 nm versus the effective diameter coarse $D_{eff,coarse}$ for the different aerosol samples
779 analysed in this study. Different symbols are used to distinguish between different aerosol types. Data
780 for both C_{ref}(W2003) and C_{ref}^{*} (multiple scattering correction obtained not taking into account the
781 shadowing effect correction in aethalometer data) are shown for ambient air aerosols, while for dust
782 and kaolinite, for which the difference between the different formulations is very low, only C_{ref}(W2003)
783 is reported. The results of the linear fits between C_{ref} and $D_{eff,coarse}$ for mineral dust and for the entire
784 dataset are also shown in the plot.

785

Atmos. Meas. Tech. Discuss., doi:10.5194/amt-2017-65, 2017
Manuscript under review for journal Atmos. Meas. Tech.
Discussion started: 18 April 2017

Atmospheric Measurement Techniques Discussions

786 **Table 1.** Specifications and references of instruments used during experiments.

Instrument	Property	Operating wavelength (nm)	Time resolution	Flowrate (L min^{-1})	Percent uncertainty	Reference
Aethalometer (model AE-31, Magee Sci.)	Spectral absorption coefficient	370, 470, 520, 590, 660, 880, 950	2 min	8	±20% (attenuation coefficient)	Hansen et al. (1984) ; W2003 ; C2010
Multi-Angle Absorption Photometer (MAAP, model 5012, Thermo Sci.)	Single-wavelength absorption coefficient	670	1 min	8	±12%	Petzold and Schönlinner (2004); Petzold et al. (2004 and 2005)
Cavity Attenuated Phase Shift Extinction (CAPS PMex, Aerodyne)	Spectral extinction coefficient	450, 630	1 s	0.85	±5%	Massoli et al. (2010)
Nephelometer (model 3563, TSI Inc.)	Spectral scattering coefficient	450, 550, 700	1 s	18	±10%	Anderson and Ogren (1998)
SMPS (DMA model 3080, CPC model 3772, TSI Inc.)	Number size distribution	–	3 min	2	–	De Carlo et al. (2004)
OPC optical particle counter (model 1.109, Grimm Inc.)	Number size distribution	655	6 s	1.2	±15% (diameter optical to geometric conversion); ±10 (concentration)	Heim et al. (2008)

787

788

Atmos. Meas. Tech. Discuss., doi:10.5194/amt-2017-65, 2017
Manuscript under review for journal Atmos. Meas. Tech.
Discussion started: 18 April 2017

Atmospheric Measurement Techniques Discussions

Table 2. Summary of experiments and results. The mean and the standard deviation of $D_{eff,fine}$, $D_{eff,coarse}$, SSA at 450 and 660 nm, C_{ref}^{*}, C_{ref}(W2003), and C_{ref}(C2010) are reported. As a reminder: C_{ref}^{*} is the multiple scattering correction obtained not taking into account the shadowing effect correction in aethalometer data; C_{ref}(W2003) and C_{ref}(C2010) take the shadowing effect correction into account, by using the parametrisations by Weingartner et al. (2003) (referred as W2003) and Collaud Coen et al. (2010) (referred as C2010), respectively. The maximum of the % difference between C_{ref}^{*}, C_{ref}(W2003), and C_{ref}(C2010) is indicated in the table.

Aerosol ID	Source	$D_{eff,fine}$ (µm) $D_{eff,coarse}$ (µm)	SSA *450 nm* 660 nm	C_{ref}^{*} *450 nm* 660 nm	C_{ref} (W2003) *450 nm* 660 nm	C_{ref} (C2010) *450 nm* 660 nm	Max % diff C_{ref} *450 nm* 660 nm
Ammonium sulfate	Sigma-Aldrich 99.999% purity	–	*0.999 ± (<)0.001* 0.999 ± (<)0.001		–	–	
Niger 1	Sahel (13.52°N, 2.63°E)	0.38 ± 0.01 2.6 ± 0.1	*0.93 ± 0.01* 0.98 ± 0.01	*2.00 ± 0.45* 1.87 ± 0.51	*2.01 ± 0.45* 1.87 ± 0.51	*2.02 ± 0.45* 1.88 ± 0.51	*1.0 %* 0.4 %
Niger 2	Sahel (13.52°N, 2.63°E)	0.32 ± 0.02 2.3 ± 0.1	*0.92 ± 0.01* 0.98 ± 0.01	*2.05 ± 0.46* 1.89 ± 0.57	*2.11 ± 0.47* 1.92 ± 0.56	*2.10 ± 0.47* 1.92 ± 0.57	*2.8 %* 1.6 %
China	Gobi desert (39.43°N, 105.67°E)	0.44 ± 0.01 3.1 ± 0.2	*0.94 ± 0.01* 0.98 ± 0.01	*2.15 ± 0.48* 2.02 ± 0.62	*2.16 ± 0.48* 2.01 ± 0.62	*2.16 ± 0.48* 2.02 ± 0.63	*0.5 %* 0.3 %
Arizona	Sonoran desert (33.15°N, 112.08°W)	0.53 ± 0.02 3.1 ± 0.2	*0.96 ± 0.01* 0.99 ± 0.01	*1.81 ± 0.40* 1.76 ± 0.56	*1.82 ± 0.41* 1.78 ± 0.55	*1.82 ± 0.41* 1.78 ± 0.57	*0.5 %* 1.1 %
Tunisia	Sahara desert (33.02°N, 10.67°E)	0.48 ± 0.03 3.2 ± 0.7	*0.96 ± 0.01* 0.99 ± 0.01	*1.97 ± 0.49* 1.80 ± 0.42	*1.98 ± 0.44* 1.80 ± 0.42	*1.98 ± 0.44* 1.80 ± 0.42	*0.5 %* 0 %
Australia	Strzelecki desert (31.33°S, 140.33°E)	0.55 ± 0.02 2.4 ± 0.1	*0.85 ± 0.01* 0.98 ± 0.01	*2.52 ± 0.56* 2.28 ± 0.74	*2.56 ± 0.57* 2.26 ± 0.72	*2.56 ± 0.57* 2.28 ± 0.74	*1.6 %* 0.9 %
Namibia	Namib desert (19.0°S, 13.0°E)	0.45 ± 0.04 3.6 ± 0.3	*0.95 ± 0.01* 0.98 ± 0.01	*2.02 ± 0.45* 1.75 ± 0.57	*2.03 ± 0.45* 1.76 ± 0.54	*2.03 ± 0.45* 1.79 ± 0.57	*0.5 %* 2.2 %
Kaolinite	Source Clay Repository KGa-2	0.39 ± 0.07 2.3 ± 1.6	*0.96 ± 0.01* 0.97 ± 0.01	*2.47 ± 0.55* 2.31 ± 0.60	*2.51 ± 0.56* 2.34 ± 0.60	*2.50 ± 0.56* 2.33 ± 0.60	*1.6 %* 1.3 %
Ambient air 1	Suburbs of Paris	0.24 ± 0.08 5.2 ± 0.9	*0.79 ± 0.05* 0.61 ± 0.08	*3.87 ± 0.87* 1.97 ± 0.71	*4.01 ± 0.90* 2.05 ± 0.73	*4.03 ± 0.90* 2.11 ± 0.76	*4.0 %* 6.6 %
Ambient air 2	Suburbs of Paris	0.50 ± 0.02 4.5 ± 0.1	*0.72 ± 0.04* 0.67 ± 0.09	*3.22 ± 0.72* 1.66 ± 0.44	*3.68 ± 0.82* 1.94 ± 0.52	*3.57 ± 0.80* 1.87 ± 0.50	*12.5 %* 14.4 %
Ambient air 3	Suburbs of Paris	0.46 ± 0.03 6.2 ± 0.7	*0.78 ± 0.06* 0.54 ± 0.10	*3.93 ± 0.88* 2.32 ± 0.76	*4.35 ± 0.97* 2.78 ± 0.89	*4.25 ± 0.95* 2.68 ± 0.87	*21.1 %* 16.5 %
Ambient air 4	Suburbs of Paris	0.53 ± 0.05 5.3 ± 1.3	*0.63 ± 0.05* 0.42 ± 0.08	*3.41 ± 0.76* 2.25 ± 0.68	*3.90 ± 0.87* 2.69 ± 0.81	*3.79 ± 0.85* 2.62 ± 0.79	*12.6 %* 16.4 %
Ambient air 5	Suburbs of Paris	0.37 ± 0.03 3.4 ± 0.1	*0.76 ± 0.08* 0.65 ± 0.12	*2.72 ± 0.61* 2.54 ± 0.82	*2.58 ± 0.58* 2.51 ± 0.81	*2.77 ± 0.62* 2.61 ± 0.85	*5.4 %* 2.7 %
Ambient air 6	Suburbs of Paris	0.37 ± 0.05 4.1 ± 1.0	*0.62 ± 0.04* 0.46 ± 0.09	*2.75 ± 0.50* 2.24 ± 0.60	*2.78 ± 0.62* 2.96 ± 0.79	*2.66 ± 0.59* 2.79 ± 0.75	*19.1 %* 24.3 %
Ambient air 7	Suburbs of Paris	0.40 ± 0.01 4.7 ± 0.7	*0.87 ± 0.05* 0.76 ± 0.08	*3.85 ± 0.86* 1.86 ± 0.74	*4.06 ± 0.91* 2.04 ± 0.69	*4.01 ± 0.90* 2.02 ± 0.80	*5.2 %* 8.8 %
Ambient air 8	Suburbs of Paris	0.42 ± 0.07 4.3 ± 0.7	*0.78 ± 0.06* 0.71 ± 0.07	*1.91 ± 0.43* 2.09 ± 0.61	*2.22 ± 0.50* 2.53 ± 0.73	*2.16 ± 0.48* 2.45 ± 0.72	*14.0 %* 17.4 %

Atmos. Meas. Tech. Discuss., doi:10.5194/amt-2017-65, 2017
Manuscript under review for journal Atmos. Meas. Tech.
Discussion started: 18 April 2017

Atmospheric Measurement Techniques Discussions

797 **Table 3**. Mean and standard deviation multiple scattering correction $\overline{C_{ref}}$ at 450 and 660 nm for dust,
798 kaolinite, and ambient air. The $\overline{C_{ref}}$ was calculated as the mean of the C_{ref}^{*}, C_{ref}(W2003), and
799 C_{ref}(C2010) obtained at each wavelength for the different aerosol types. As a reminder: C_{ref}^{*} is the
800 multiple scattering correction obtained not taking into account the shadowing effect correction in
801 aethalometer data; C_{ref}(W2003) and C_{ref}(C2010) take the shadowing effect correction into account, by
802 using the parametrisations by Weingartner et al. (2003) and Collaud Coen et al. (2010), respectively.

803

	$\overline{C_{ref}}$	
	450 nm	**660 nm**
Mineral dust	2.09 ± 0.22	1.92 ± 0.17
Kaolinite	2.49 ± 0.02	2.32 ± 0.01
Ambient air	3.31 ± 0.75	2.32 ± 0.35

804

805

Atmos. Meas. Tech. Discuss., doi:10.5194/amt-2017-65, 2017
Manuscript under review for journal Atmos. Meas. Tech.
Discussion started: 18 April 2017

Atmospheric Measurement Techniques Discussions

806 **Figure 1.** Experimental setup used for the aethalometer intercomparison experiments.

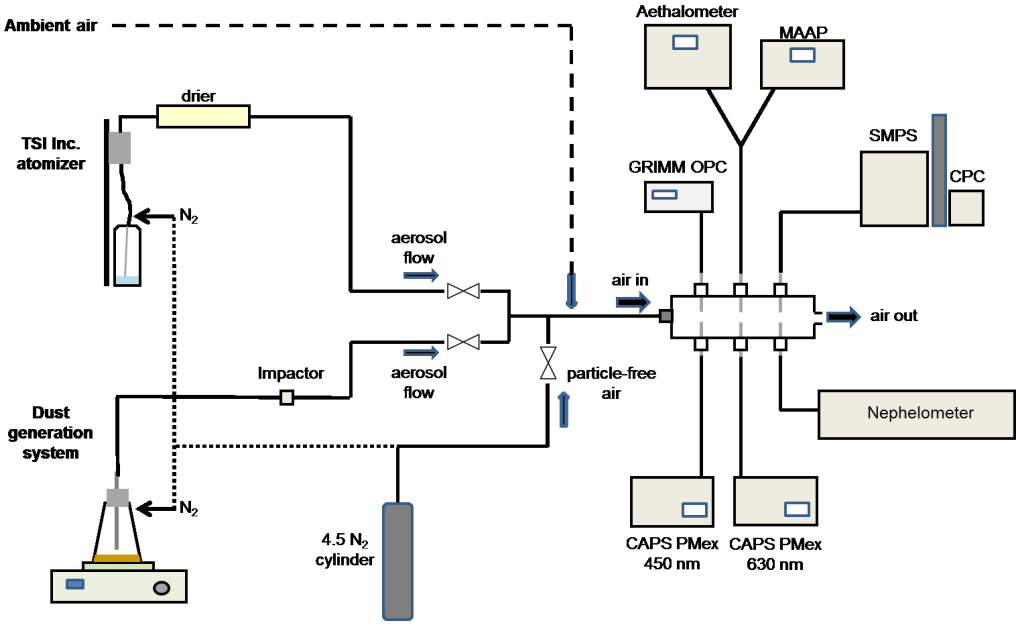

807
808

809

810

Atmos. Meas. Tech. Discuss., doi:10.5194/amt-2017-65, 2017
Manuscript under review for journal Atmos. Meas. Tech.
Discussion started: 18 April 2017

Atmospheric Measurement Techniques Discussions

811 **Figure 2.** Temporal series of experiments showing the measured optical data at 660 nm. The different
812 panels show (from the top to the bottom): (i) the shadowing-corrected aethalometer attenuation at 660
813 nm (data corrected with the R formulation by Collaud Coen et al. (2010) (referred as R(C2010)) are
814 shown) and the MAAP aerosol absorption coefficient; (ii) the aerosol extinction at 660 nm
815 extrapolated from CAPS PMex measurements and estimated as the sum of nephelometer scattering
816 and MAAP absorption; (iii) the extinction aerosol Ángstrom exponent; (iv) the aerosol single scattering
817 albedo at 660 nm. Each point in the plot corresponds to 2 min average data. The x-axis indicates the
818 data point sequential number. Experiments with dust samples and kaolinite were realised between the
819 3rd and the 9th of November 2016 and lasted between 1 and 2 hours each. Ambient air data were
820 collected at different steps between the 8th and the 14th November 2016 for a total of 7 hours of
821 measurements.

822

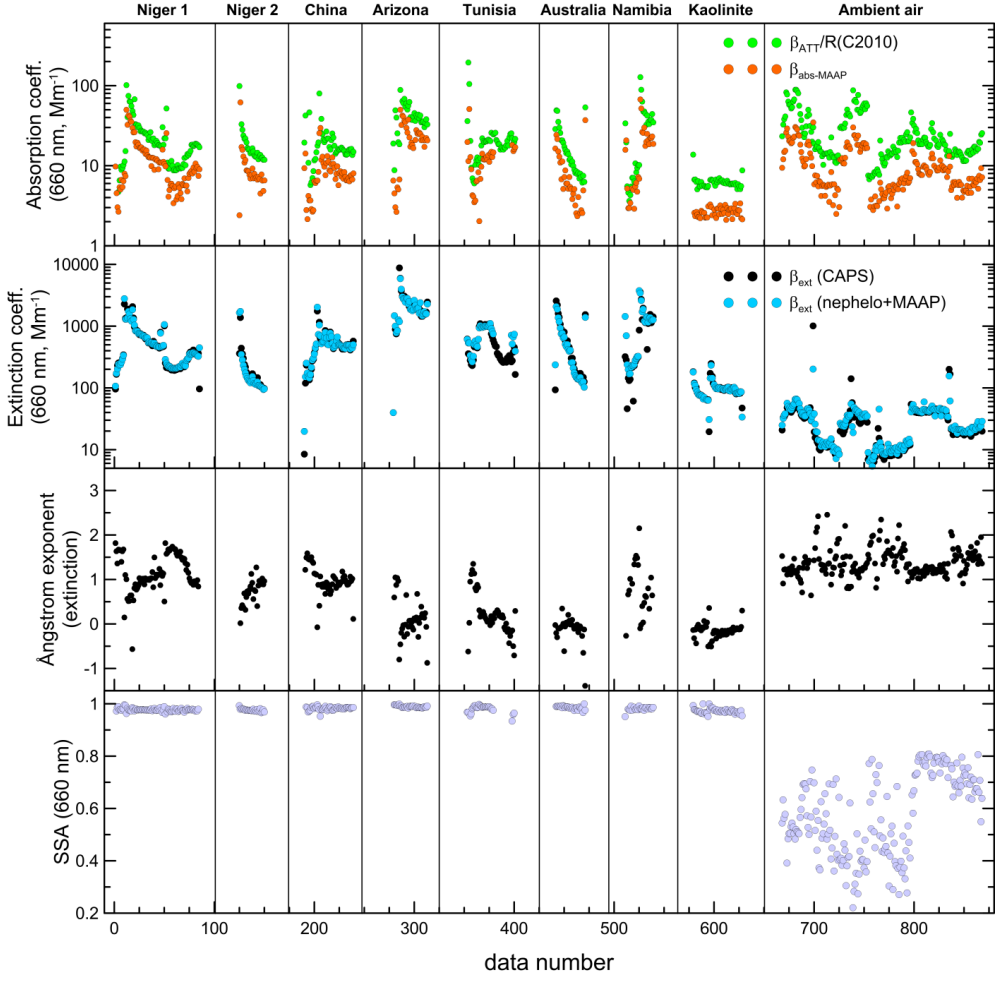

823
824

Atmos. Meas. Tech. Discuss., doi:10.5194/amt-2017-65, 2017
Manuscript under review for journal Atmos. Meas. Tech.
Discussion started: 18 April 2017

Atmospheric Measurement Techniques Discussions

825 **Figure 3.** Ammonium sulfate experiment. Left panel: temporal evolution of the extinction and
826 scattering coefficients measured by the CAPS PMex and the nephelometer at 450 nm (blue scale)
827 and 630 nm (red scale). Each point in the plot corresponds to 2 min average data. Right panel: CAPS
828 PMex versus nephelometer data (10 minutes averages). The y=x line and the results of the linear fit
829 between CAPS and nephelometer data are also shown in the plot.

830

831

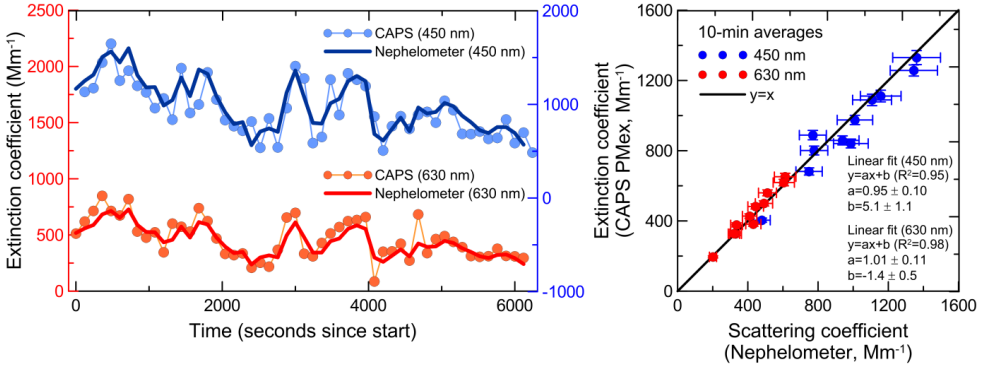

832

833

834 **Figure 4.** CAPS PMex extinction coefficient extrapolated at 660 nm versus nephelometer+MAAP
835 calculated extinction at 660 nm for all experiments (dust, kaolinite, ambient air). Each point in the plot
836 corresponds to 10 min average data. The y=x line and the results of the linear fit between CAPS and
837 nephelometer+MAAP data are also shown in the plot.

838

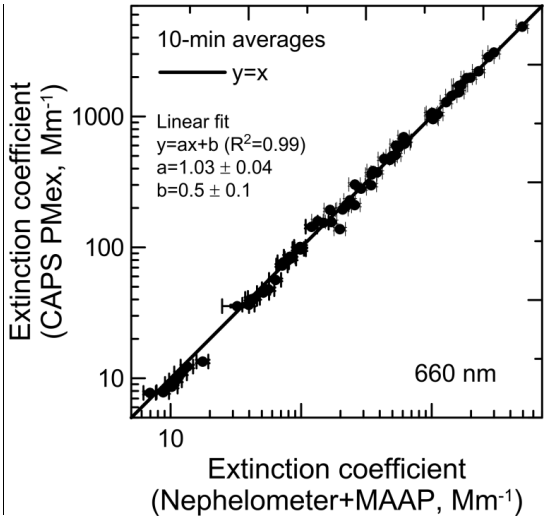

839
840
841
842
843
844
845
846
847
848
849
850
851
852
853
854

855 **Figure 5.** Left panel: estimated f values versus (1-SSA) at 660 nm for dust aerosols. Different
856 symbols are used to distinguish between dust from different sources. Right panel: f versus SSA at

Atmos. Meas. Tech. Discuss., doi:10.5194/amt-2017-65, 2017
Manuscript under review for journal Atmos. Meas. Tech.
Discussion started: 18 April 2017

Atmospheric Measurement Techniques Discussions

857 660 nm for all experiments. Different symbols are used to distinguish between different aerosol types.
858 The results of the linear fit between f and (1-SSA) are also reported. Data from Weingartner et al.
859 (2003) (W2003) (extracted from their Figure 4) are also shown in the plot for comparison.

860

861

862

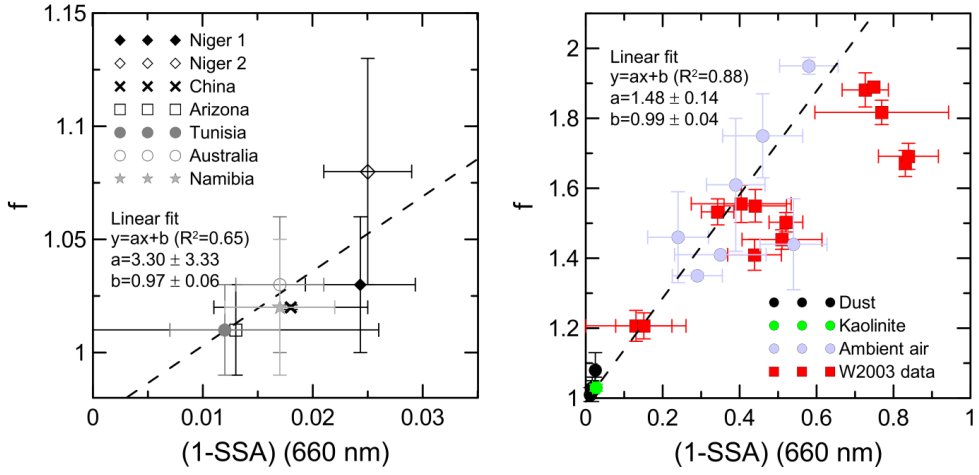

863

864

Atmos. Meas. Tech. Discuss., doi:10.5194/amt-2017-65, 2017
Manuscript under review for journal Atmos. Meas. Tech.
Discussion started: 18 April 2017

Atmospheric Measurement Techniques Discussions

865 **Figure 6.** Top panel: C_{ref}(W2003) (multiple scattering correction obtained by taking into account the
866 shadowing effect correction using the parametrisations by Weingartner et al. (2003)) versus SSA at
867 450 and 660 nm for mineral dust samples analysed in this study. Different symbols are used to
868 distinguish between dust from different sources. As indicated in Table 2, the difference between C_{ref}^{*},
869 C_{ref}(W2003), and C_{ref}(C2010) is very low for mineral dust aerosols. Bottom panel: C_{ref} versus SSA at
870 450 and 660 nm for the different aerosol samples analysed in this study. Different symbols are used
871 to distinguish between different aerosol types. Data for both C_{ref}(W2003) and C_{ref}^{*} (multiple scattering
872 correction obtained not taking into account the shadowing effect correction in aethalometer data) are
873 shown for ambient air aerosols, while for dust and kaolinite, for which the difference between the
874 different formulations is very low, only C_{ref}(W2003) is reported. Data from Weigartner et al. (2003)
875 (W2003) (C_{ref} from their Table 3, and SSA extracted from their Fig. 4) and Collaud Coen et al. (2010)
876 (C2010) (extracted from their Fig. 5) at 660 nm are also shown in the plot for comparison. The results
877 of the linear fits between C_{ref} and SSA for mineral dust and for the entire dataset are also shown in the
878 plot.

879

880

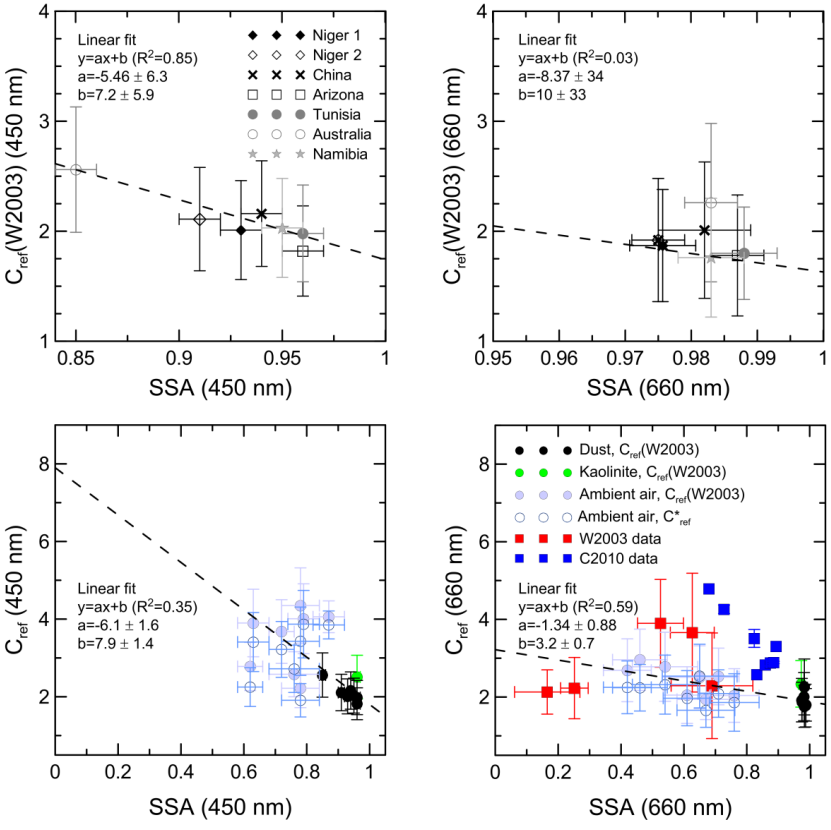

881

882

Atmos. Meas. Tech. Discuss., doi:10.5194/amt-2017-65, 2017
Manuscript under review for journal Atmos. Meas. Tech.
Discussion started: 18 April 2017

Atmospheric Measurement Techniques Discussions

883 **Figure 7.** Examples of number size distribution (normalised to the total number concentration) for
884 ammonium sulfate, dust (Niger sample), kaolinite, and ambient air aerosols. Data refer to the mean
885 over each experiment as measured from the SMPS and the OPC. Error bars (standard deviations)
886 have been omitted for the sake of clarity.

887

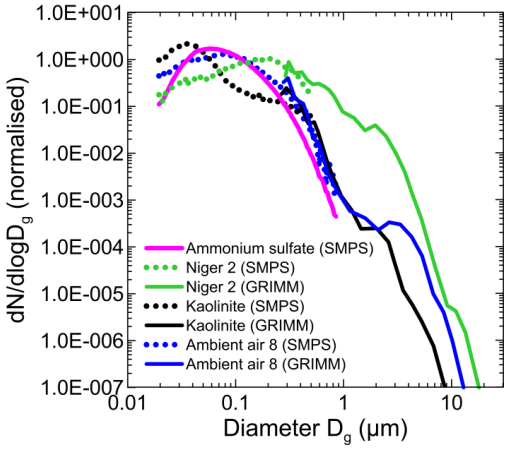

888

889

Atmos. Meas. Tech. Discuss., doi:10.5194/amt-2017-65, 2017
Manuscript under review for journal Atmos. Meas. Tech.
Discussion started: 18 April 2017

Atmospheric Measurement Techniques Discussions

Figure 8. Top panel: C_{ref}(W2003) (multiple scattering correction obtained by taking into account the shadowing effect correction using the parametrisations by Weingartner et al. (2003)) at 450 and 660 nm versus the effective diameter coarse $D_{eff,coarse}$. for mineral dust samples analysed in this study. Different symbols are used to distinguish between dust from different sources. Bottom panel: C_{ref} at 450 and 660 nm versus the effective diameter coarse $D_{eff,coarse}$ for the different aerosol samples analysed in this study. Different symbols are used to distinguish between different aerosol types. Data for both C_{ref}(W2003) and C_{ref}^{*} (multiple scattering correction obtained not taking into account the shadowing effect correction in aethalometer data) are shown for ambient air aerosols, while for dust and kaolinite, for which the difference between the different formulations is very low, only C_{ref}(W2003) is reported. The results of the linear fits between C_{ref} and $D_{eff,coarse}$ for mineral dust and for the entire dataset are also shown in the plot.